



High Voltage Stable Li Metal Batteries Enabled by Ether-Based Highly Concentrated Electrolytes at Elevated Temperatures

Yongjun Leng,^{*}  Shanhai Ge, Ryan S. Longchamps,  Xiao-Guang Yang, Teng Liu,^{**} and Chao-Yang Wang^{*,z} 

Electrochemical Engine Center and Department of Mechanical Engineering, Pennsylvania State University, University Park, Pennsylvania 16802, United States of America

Li metal batteries (LMBs) employing high voltage cathodes are necessary to attain high energy density. Although highly concentrated ether-based electrolytes (e.g. 4 M LiFSI/DME) can yield stable cycling of Li metal anodes, their high voltage instability fosters incompatibility with high voltage cathodes. In this work, the temperature dependence of fresh cell performance, Li Coulombic efficiency (CE), and cycling stability of LMBs in highly concentrated LiFSI/DME electrolytes was explored. Elevated temperature operation was deemed essential for highly concentrated electrolytes to achieve practical rate capability. Moreover, at 60 °C, the cycling stability of Li metal anodes with a Li CE as high as 99.2% was demonstrated in a highly concentrated LiFSI-1.2DME electrolyte (LiFSI: DME = 1: 1.2 mol.). At room temperature, the LiFSI-1.2DME electrolyte enabled stable LMBs with NMC622 cathodes. However, due to the high temperature and high voltage instability of the LiFSI-1.2DME electrolyte in contact with NCM622, a small amount of TAP (~1 wt.%) was added, significantly enhancing the cycling stability at 60 °C. This newly developed LiFSI-1.2DME electrolyte with 1 wt.% TAP ultimately enabled LMBs with NMC622 cathodes and minimal excess Li metal anode to be cycled stably for 200–300 cycles at 60 °C.

© 2020 The Electrochemical Society ("ECS"). Published on behalf of ECS by IOP Publishing Limited. [DOI: [10.1149/1945-7111/aba513](https://doi.org/10.1149/1945-7111/aba513)]

Manuscript submitted May 5, 2020; revised manuscript received June 16, 2020. Published July 21, 2020.

Supplementary material for this article is available [online](#)

Beyond fast rechargeability, safety and cost, range anxiety is one of the major obstacles that hinders the widespread adoption of battery electric vehicles (BEVs).^{1–3} In general, the range of BEVs is mainly limited by the energy densities of commercially available Li-ion batteries with graphite anodes. To address this issue, it is desirable to develop next-generation batteries with leapfrogging increase in energy density for the use in BEVs. Since Li metal has the highest theoretical capacity (3,860 mAh g⁻¹) and lowest electrochemical potential (–3.04 V vs standard hydrogen electrode), it has been regarded as the best choice as the anode in next-generation batteries with high energy density to pair with Li-layer oxide cathode, Li-sulfur, and Li-air batteries.^{4,5} Coupled with high capacity layer oxide cathodes such as Ni-rich Li(Ni_xMn_yCo_z)O₂ (x + y + z = 1, x > 0.5) (NMC), the replacement of graphite anodes in state-of-the-art Li-ion batteries by Li metal anodes can boost the energy density of the batteries from its current state, <250 Wh kg⁻¹, to 350–500 Wh kg⁻¹.^{5,6} However, low Li Coulombic efficiency stemming from parasitic reactions between Li metal and liquid electrolytes and safety concerns due to uncontrolled Li dendrite formation/growth have hindered the practical use of Li metal anodes. Recently, several strategies have been proposed to increase the Li Coulombic efficiency and/or suppress Li dendrite formation/growth, including Li surface protection,^{7–11} three dimensional host/matrix implementation,^{12–15} Li alloying with other elements,^{16–18} development of artificial solid-electrolyte interphase (SEI) layer on Li metal,^{19–23} modification of liquid electrolyte formula,^{24–26} and adoption of highly concentrated electrolytes.^{27–31}

Compared to conventional dilute electrolytes, highly concentrated electrolytes (HCEs) (usually >3–5 M depending on salt-solvent combinations) have been receiving much attention for stable Li metal anodes in recent years due to their unique physicochemical and electrochemical properties.^{27,32} In HCEs, most solvents are solvated with Li ions, leaving a very small amount of free solvents. This significantly reduces side reactions between Li metal and solvents and thus achieves a high Li Coulombic efficiency. Moreover, the SEI layer formed on Li metal in the presence of HCEs is derived from the reduction of salts rather than solvents. This

kind of anion-derived SEI is robust and effective for suppressing Li dendrite formation/growth. A number of solvents such as 1,2-dimethoxyethane (DME), dimethyl carbonate (DMC), sulfolane (SL) and triethyl phosphate (TEP), together with several type of Li salts such as lithium bis(fluorosulfonyl)imide (LiFSI), lithium bis(trifluoromethanesulfonyl)imide (LiTFSI) and lithium difluoro(oxalate)borate (LiDFOB), were explored to form HCEs for stable dendrite-free Li metal anodes, such as LiFSI/DME,^{29,33,34} LiFSI/DMC,^{27,28,35} LiFSI/SL,³⁶ LiTFSI-LiDFOB/DME,³⁷ and LiFSI/TEP.³⁸ Compared with other solvents, ether-based HCEs such as LiFSI/DME have demonstrated better compatibility with Li metal and high Li Coulombic efficiency of up to 99.1%.²⁹ However, ether-based electrolytes have often been used in Li metal batteries (LMBs) with low voltage (<4.0 V) cathodes such as Li || LiFePO₄, Li || sulfur and Li || O₂ since ether solvents are believed to be unstable at high voltages of >4.0 V (vs Li/Li⁺).^{33,37} Recently, several studies have reported the exploration of ether-based HCEs for LMBs with high voltage cathodes.^{34,37,39} For example, Jiao et al.³⁷ adopted a bi-salt (LiTFSI-LiDFOB) DME-based HCE for a LMB consisting of 250 μm thick Li metal anode and a LiNi_{0.4}Mn_{0.4}Co_{0.2}O₂ (NMC442) cathode with an active mass loading of 10.8 mg cm⁻² and achieved ~500 stable cycles at a capacity retention of 80% at room temperature (RT). Alvarado et al.³⁹ reported that a LMB consisting of 150 μm thick Li metal anode and a LiNi_{0.6}Mn_{0.2}Co_{0.2}O₂ (NMC622) cathode with an areal capacity of 1.44 mAh cm⁻² can achieve >300 stable cycles using a bi-salt (LiTFSI-LiFSI) DME-based HCE at RT. Thus, there may exist a possibility for a viable, high-voltage LMB utilizing an ether-based electrolyte.

Since the ionic conductivity and Li ion diffusion coefficient of HCEs are much lower than conventional dilute electrolytes at RT,^{27,29,31} the rate performance of LMBs with HCEs is typically poor. Therefore, in the literature, most LMBs with HCEs are operated at low charge/discharge current density, limiting their utility. At elevated temperatures such as 60 °C, the ionic conductivity and Li ion diffusion coefficient of HCEs increase significantly.³¹ Thus, an attendant improvement in rate performance of LMBs is expected under these conditions. Moreover, at elevated temperatures, enhanced Li ion mass transport may promote the smooth deposition of Li during the charge step, avoiding the Li dendrite formation/growth and thus improving Li Coulombic efficiency. Recently, Cui's group⁴⁰ reported the improving cyclability

*Electrochemical Society Member.

**Electrochemical Society Student Member.

^zE-mail: cxw31@psu.edu

of LMBs and a high Li Coulombic efficiency of 99.3% for an ether-based electrolyte of 1 M LiTFSI/DOL-DME with 1 wt.% LiNO₃ at 60 °C. Unfortunately, at elevated temperatures, the degradation of LMBs may also accelerate due to enhanced side reactions between electrolytes and cathode materials at high voltages, especially when highly active Ni-rich NMC cathode materials are employed. Xia's group⁴¹ investigated the Li Coulombic efficiency of the LiTFSI/DOL-DME (1:1 vol.%) with 2 wt.% LiNO₃ electrolytes with different salt concentrations and found that a higher concentration electrolyte (such as 3–5 M) can improve Li Coulombic efficiency, and a higher temperature (such as 60 °C) can help Li plate/strip uniformly with less Li dendritic growth. However, they focused their work on Li metal anodes and demonstrated the performance of Li metal batteries with low-voltage lithium iron phosphate (LFP) cathodes.

In this report, we implement highly concentrated LiFSI/DME electrolytes with high salt/solvent molar ratios combined with a suitable electrolyte additive to enhance the stability of ether-based HCEs at both high voltages and high temperatures. Specifically, we demonstrate stable LMBs with high voltage NMC622 cathodes in highly concentrated LiFSI/DME electrolytes combined with triallyl phosphate (TAP) electrolyte additive at 60 °C. TAP is used as the electrolyte additive due to its proven ability to increase the stability of graphite-NMC cells operating at both high-voltage and high-temperature conditions.^{42,43}

Experimental

Materials and electrolyte preparation.—Battery-grade LiFSI salt was supplied by Nippon Shokubai, Japan. DME solvent and TAP were sourced from Sigma-Aldrich and TCI American, respectively. Li chips with a thickness of 250 μm were purchased from MTI Corporation; while Li discs were cut from 20 μm thick Li foils coated on 10 μm thick Cu foils purchased from Uniglobe Kisco, Japan. All electrolytes were prepared in an Ar-filled MBraun glove box with an oxygen level of <0.1 ppm and H₂O level of <0.1 ppm. The electrolytes were prepared by dissolving LiFSI salt in the DME solvent under mechanical stirring. The LiFSI/DME molar ratio for the two different electrolytes is 1/2.4 (denoted as LiFSI-2.4DME, ~3.0 M LiFSI based on total volume of salt and solvent) and 1/1.2 (denoted as LiFSI-1.2DME, ~4.9 M LiFSI), respectively. To prepare an electrolyte with TAP additive, 1 wt.% TAP was added into the LiFSI-1.2DME electrolyte under stirring. NMC622 cathodes were fabricated with active material loading of 10.5 mg cm⁻² on 15 μm Al foil.

Coin cell preparation.—Each Li || Cu coin cell consisted of a Li chip with a thickness of 250 μm and a diameter of 9 mm, a layer of Celgard-2325 separator with a thickness of 25 μm, and a piece of Cu disc with a thickness of 10 μm and a diameter of 19 mm. The Li || Cu coin cells were assembled inside a glove box using CR2032 type coin cell cases with the corresponding conventional spacers and springs (MTI Corporation). Each Li || NMC622 coin cell consisted of a Li anode, a layer of Celgard-2325 separator with a thickness of 25 μm, and a NMC622/Al foil disc with a diameter of 14 mm as a cathode. The Li anode used was either a Li chip with a thickness of 250 μm and a diameter of 15.8 mm or a Li disc with a thickness of 20 μm and a diameter of 15–16 mm cut in-house. CR2032-type Li || NMC622 coin cells were assembled inside glove box using CR2032-type coin cell cases (Hohsen, Japan) with spacers and springs (MTI Corporation). Al-cladded cathode cases were used to avoid the corrosion of stainless steel at high voltages. For each Li || Cu or Li || NMC622 coin cell, approximately 100 μl of electrolyte was used.

Electrochemical characterization.—For the measurement of Li Coulombic efficiency in the Li || Cu coin cells, Li was first electroplated onto the Cu foil at a prescribed current density for a required time to achieve a required plating capacity, and then the deposited Li was stripped from Cu foil until a cut-off voltage of

–1.0 V vs Li/Li⁺ was reached. The plating/stripping cycle was repeated for a number of cycles sufficient for determining the Li Coulombic efficiency. For fresh Li || NMC622 coin cells, after several formation cycles, the C/10 performance characterization of the fresh cells was performed using C/10 charge and C/10 discharge between 2.8 and 4.3 V at either RT or 60 °C. During the C/10 performance characterization, an additional constant voltage (CV) step was added to the charging process, and the cells were kept at 4.3 V until the current was lower than C/20. After C/10 performance characterization, the coin cells were cycled at a required C-rate between 2.8 and 4.3 V at RT (C/3 charge and C/3 discharge) or 60 °C (C/3 charge and 1C discharge). An additional CV step was also added to the charging process during cycling, during which the cells were kept at 4.3 V until the current was lower than C/10. The current densities corresponding to all C-rates were calculated based on the actual capacity of each respective fresh coin cell obtained from the C/10 performance characterization. The cycling test was interrupted after a certain number of cycles (typically every 100 cycles) for the C/10 performance characterization (as reference performance test) and the electrochemical impedance spectroscopy (EIS) test. All electrochemical tests were carried out using either a Land battery testing system (Model: CT2001A, Wuhan Land, China) or an Arbin battery testing system (Model: BT2000, Arbin, USA). The C/10 performance of the aged cells was evaluated between 2.8 and 4.3 V using the same method as for the fresh cells. For the EIS measurement of fresh and aged cells, the cells were fully charged to 4.3 V using a C/10 rate before being discharged to a state of charge (SoC) of 90% using a C/10 rate. The EIS measurement was performed using a Modulab testing system (Ametek Scientific Instrument, USA) with a frequency range of 1 M to 0.01 Hz and ac amplitude of ±5 mV at RT or 60 °C.

Results and Discussion

Temperature effect on the performance of fresh Li || NMC622 coin cells.—Figure 1a shows the performance of fresh Li || NMC622 coin cells under C/10 charge/discharge at RT and 60 °C. At RT, the cells delivered a C/10 discharge capacity of ~160 and ~156 mAh g⁻¹ NMC622 in LiFSI-2.4DME and LiFSI-1.2DME electrolytes, respectively. The C/10 discharge capacity at RT is substantially lower than typical reported values of 180–190 mAh g⁻¹.⁴⁴ This discrepancy results from the low ionic conductivities and low Li ion diffusion coefficients of HCEs at RT.^{27,29,31} At 60 °C, the cells delivered a discharge capacity under C/10-rate of ~186 and ~188 mAh g⁻¹ NMC622 in LiFSI-2.4DME and LiFSI-1.2DME electrolytes, respectively, which is ~16.3% and ~20.5% higher than that at RT and in agreement with previously reported intrinsic NMC622 capacities. This means that the cells in the same HCEs can deliver at least 16.3%–20.5% higher energy density at 60 °C than at RT. The increase in specific C/10 discharge capacity and energy density is due to the increase in the ionic conductivity, decreased viscosity, and high Li ion diffusion coefficient of HCEs at elevated temperatures.³¹ Moreover, at 60 °C, with the addition of 1 wt.% TAP into LiFSI-1.2DME electrolyte, the C/10 charge/discharge voltage profile remains unchanged, and the cell delivers almost the same discharge capacity and energy density as the case of the pure electrolyte. The performance of fresh Li || NMC622 coin cells under higher charge/discharge rates at RT and 60 °C was also investigated in the LiFSI-1.2DME electrolyte without and with 1 wt.% TAP. As shown in Fig. 1b, at RT, the cell in pure LiFSI-1.2DME electrolyte demonstrates higher charge potential and lower discharge potential under C/3-rate than that under C/10. This means the rate capability of the cell with HCE is poor at RT. Furthermore, the cell at RT in pure LiFSI-1.2DME electrolyte delivers a C/3 discharge capacity of ~148 mAh g⁻¹, which is ~94.9% of C/10 discharge capacity. However, at 60 °C, the cell in pure LiFSI-1.2DME electrolyte demonstrates slightly higher charge potential under C/3-rate charge and slightly lower discharge potential under 1C-rate discharge when compared to the C/10 case. This indicates the rate capability of the cell with HCE is improved at elevated

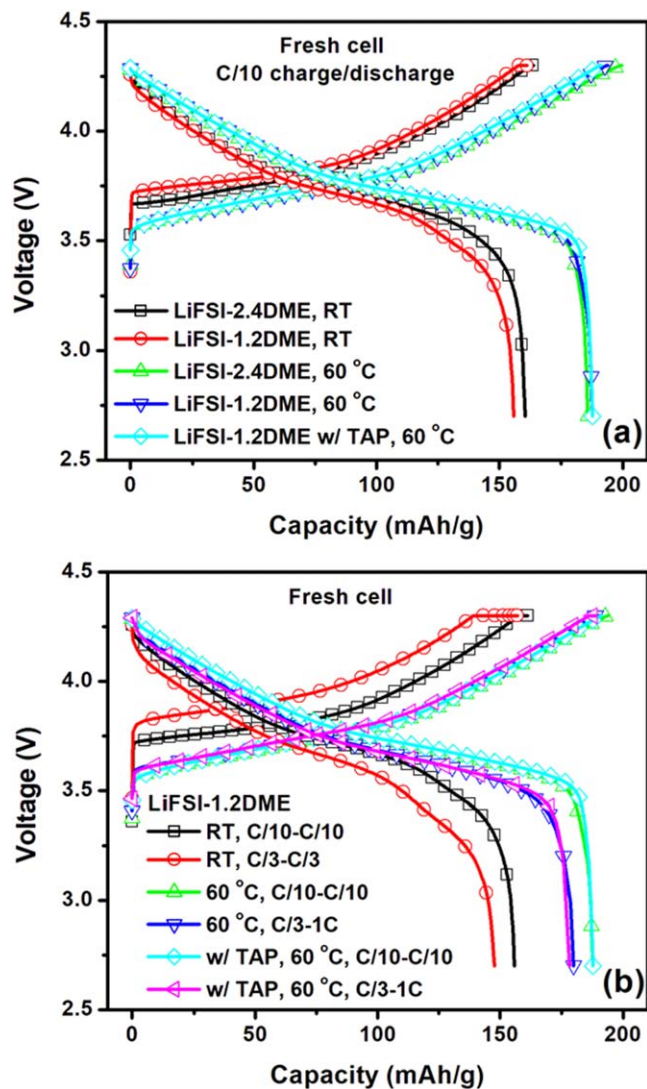


Figure 1. Performance of fresh Li (250 μm thick) || NMC622 under different C-rate in three types of electrolytes: LiFSI-2.4DME, LiFSI-1.2DME and LiFSI-1.2DME w/1 wt.% TAP at RT and 60 °C: (a) C/10 charge/discharge at RT and 60 °C, (b) C/3 charge/C/3 discharge at RT and C/3 charge/1C discharge at 60 °C.

temperatures. The cell in pure LiFSI-1.2DME electrolyte delivered a discharge capacity of $\sim 180 \text{ mAh g}^{-1}$ even under 1C-rate at 60 °C, which is $\sim 21.6\%$ higher than that of the C/3 case at RT. Moreover, with the addition of TAP into the LiFSI-1.2DME electrolyte, the cell delivered almost the same discharge capacity under 1C-rate as the case of the pure electrolyte.

Figure 2 shows the impedance spectra of the fresh Li || NMC622 coin cells under 90% State-of-charge (SoC) at RT and 60 °C in the LiFSI-1.2DME electrolyte without and with 1 wt.% TAP. In both cases, the increase of operating temperature from RT to 60 °C significantly decreases the total cell resistance (excluding the part related to the diffusion line). For example, the total cell resistance at 60 °C is ~ 6.1 and $\sim 7.2 \text{ ohm cm}^2$ in the LiFSI-1.2DME electrolyte without and with 1 wt.% TAP, respectively, which represents a 77% and 72% reduction in resistance for each respective electrolyte at RT. The significant decrease in the total cell resistance at elevated temperatures results from the increased ionic conductivity of HCEs and enhanced kinetics of the electrochemical reactions at the Li metal-HCE and NMC622-HCE interfaces. Ultimately, this yields enhanced rate capability and improved C/10 charge/discharge performance as observed in Fig. 1.

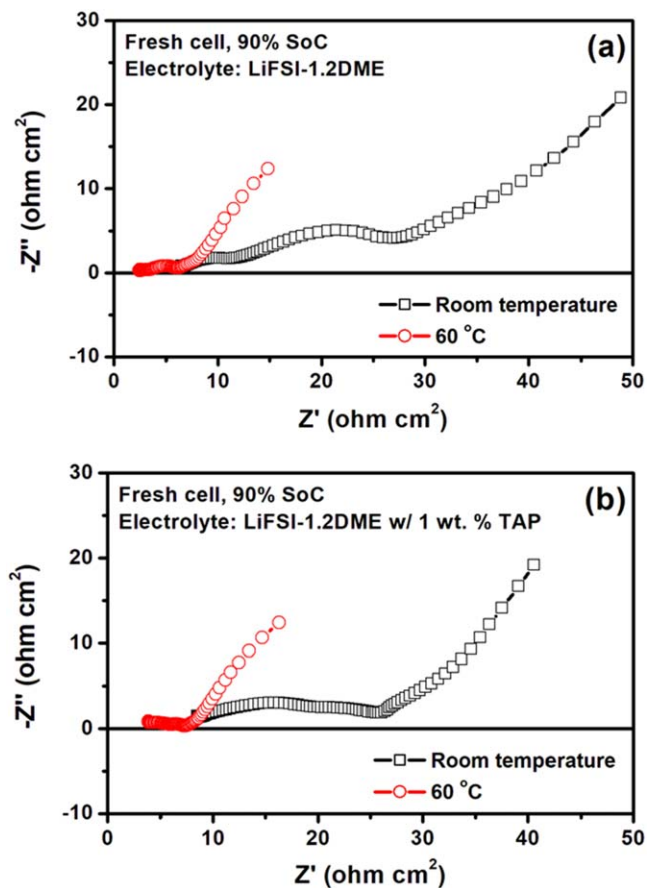


Figure 2. Effect of temperature on the impedance of fresh Li || NMC622 coin cells at 90% SoC in different electrolytes: (a) LiFSI-1.2DME, and (b) LiFSI-1.2DME with 1 wt.% TAP.

Effect of temperature on Li Coulombic efficiency.—Li Coulombic efficiency (CE) is a crucial factor in the cycle life of LMBs, indicative of the rate at which the Li metal anode is consumed. Li CE is especially important when Li metal anodes of limited excess Li (i.e. 20–50 μm thickness) are used.^{45,46} In order to achieve a decent cycle life for LMBs, a CE of $>99\%$ is required. With this target in mind, Li || Cu coin cells were used to investigate the stability of repetitive Li plating/stripping through the measurement of Li CE. The CE is defined as the ratio of the capacity of Li stripped from Cu substrate to that plated on Cu substrate during the same cycle. Figure 3 shows CE evolution with cycle number in three types of ether-based electrolytes: LiFSI-2.4DME, LiFSI-1.2DME, and LiFSI-1.2DME with 1 wt.% TAP at RT, 40 °C, and 60 °C. The current density applied for plating/stripping is 1 mA cm^{-2} , and the total plating capacity is 2 mAh cm^{-2} , which is close to the areal capacity of NMC622 cathodes used in this work. For all nine temperature-electrolyte cases, the CE gradually increases with cycle number within the first 100 cycles. After 100 cycles, a quite stable value of CE is achieved for more than 300–400 cycles, depending on the electrolyte type and operating temperature. During the final stage of long-term plating/stripping cycling, there are some data points that deviate from the average value of $\sim 99\%$ by several percent. These points indicate the possible breakup of the SEI layer formed on Li metal and/or existence of soft Li internal shorting due to the formation/growth of Li dendrites after the long-term cycling. The average CE during the initial 400 cycles is calculated for all nine cases and shown in Fig. 4, except for the case of LiFSI-2.4DME electrolyte at RT where the average CE is calculated during the initial 290 cycles due to the early onset of significant CE variation/instability around cycle 300. For LiFSI-2.4DME electrolyte, the

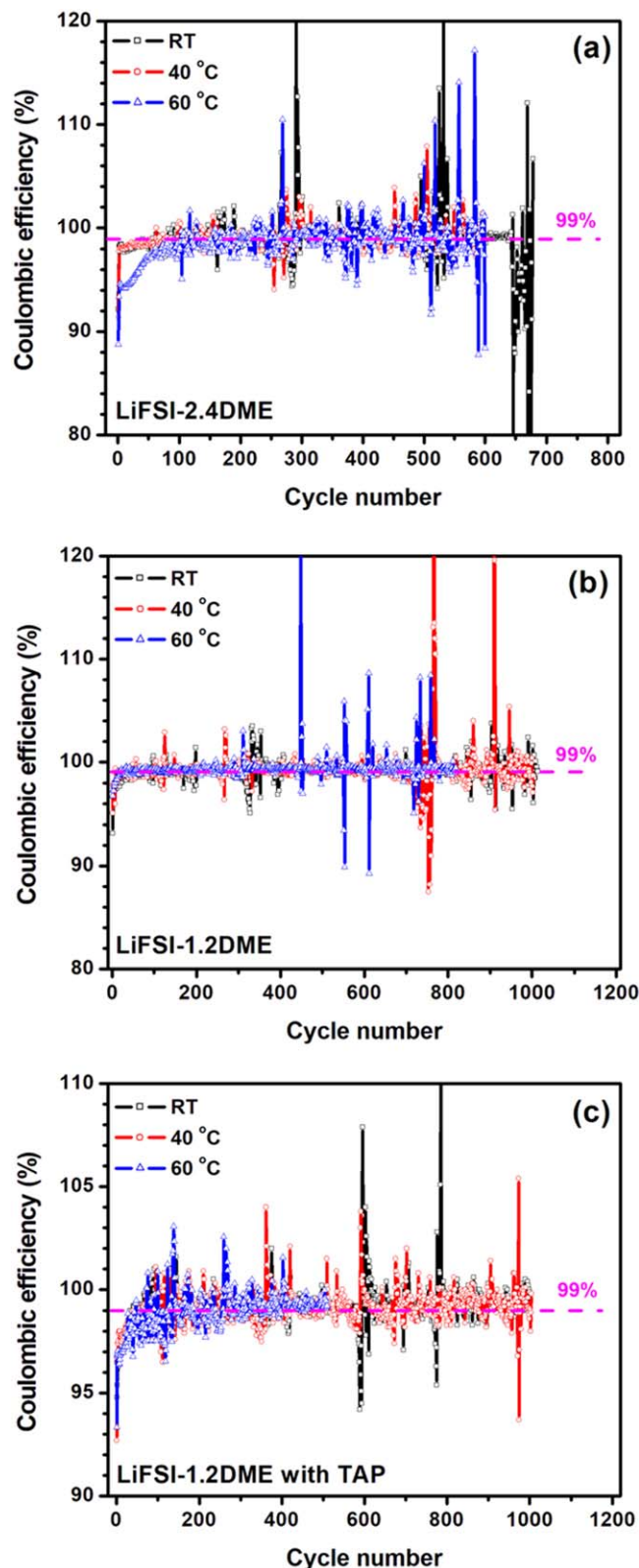


Figure 3. Stability of Li Coulombic efficiency with cycling measured under a plating/stripping current density of 1 mA cm^{-2} and a plating capacity of 2 mAh cm^{-2} in Li || Cu cells with different ether-based electrolytes: (a) LiFSI-2.4DME, (b) LiFSI-1.2DME, and (c) LiFSI-1.2DME with 1 wt.% TAP.

average CE under a current density of 1 mA cm^{-2} and an areal plating capacity of 2 mAh cm^{-2} for initial 290 cycles is 98.6% at RT, which is very close to the value ($\sim 98.5\%$) under 1 mA cm^{-2}

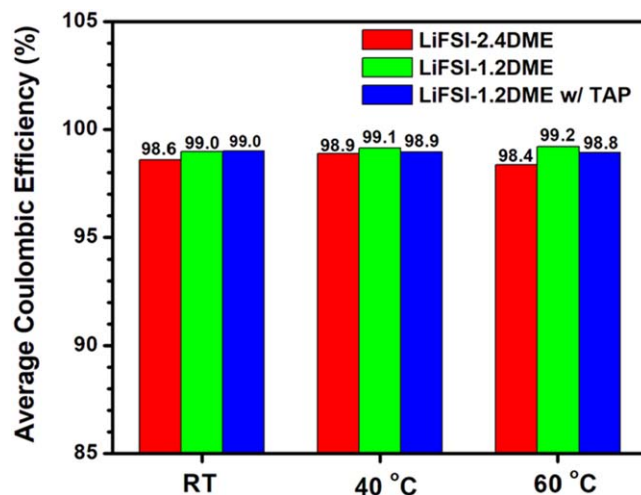


Figure 4. Average Li Coulombic efficiency during initial 400 cycles measured under a plating/stripping current density of 1 mA cm^{-2} and a plating capacity of 2 mAh cm^{-2} in Li || Cu cells with different ether-based electrolytes (Except for the case of LiFSI-2.4DME at room temperature (RT), the average CE is calculated during initial 290 cycles).

and 0.5 mAh cm^{-2} for a LiFSI/DME electrolyte with a similar salt/solvent ratio ($\sim 4 \text{ M}$) reported by Qian et al.²⁹ With an increase in temperature from RT to 40 and 60 °C, the average CE in LiFSI-2.4DME electrolyte changes slightly with temperature. Moreover, when the salt/solvent molar ratio increases from 1/2.4 (i.e. LiFSI-2.4DME) to 1/1.2 (i.e. LiFSI-1.2DME), the CE slightly increases at all three temperatures. This result is expected due to the reduced presence of free solvent in the case of the higher salt concentration electrolyte, which limits solvent-Li metal side reactions and increases the CE. The average CE for the initial 400 cycles in LiFSI-1.2DME electrolyte is 99.0, 99.1 and 99.2% at RT, 40, and 60 °C, respectively. With the addition of 1 wt.% TAP into the LiFSI-1.2DME electrolyte, the average CE for the initial 400 cycles slightly decreases, especially at elevated temperatures such as 60 °C. For reference, it is useful to note that the CE in all three electrolytes is much higher than a conventional dilute liquid electrolyte such as 1 M LiPF₆ in EC/EMC + 2% VC at RT and 60 °C (Fig. S1 is available online at stacks.iop.org/JES/167/110543/mmedia). Figure 4 also reveals a slight variation in CE with temperature for all three types of electrolyte unlike the observation reported by Cui's group for a 1 M LiTFSI/DOL-DME + 1 wt.% LiNO₃ electrolyte.⁴⁰ This may be due to the use of a different solvent and salt concentration in this work. Cui's group also reported that for some electrolytes, the average CE slightly increases with temperature; while for some other electrolytes, the average CE significantly decreases with temperature.⁴⁰ We believe that there are two primary factors affecting the CE at elevated temperatures: (1) Li ion mass transport is enhanced, reducing and/or avoiding the formation/growth of Li dendrites and leading to larger Li particle size deposition on the Li metal anode thus shrinking the electrolyte/electrode interfacial area and increasing the CE,⁴⁰ and (2) the kinetics of the undesirable reactions between the Li metal and solvent accelerates, which decreases the CE. Therefore, the temperature dependence of CE relies on the net effect of these two competing factors, which may vary among different electrolytes.

We also investigated the stability of CE with cycling under higher current density and plating capacity in the highly concentrated LiFSI-1.2DME electrolyte at 60 °C, as shown in Fig. 5a. For all three current density and plating capacity conditions, the CE is stable for at least 400 cycles similar to the 1 mA cm^{-2} and 2 mAh cm^{-2} case for the same electrolyte at 60 °C. The average CE for the first 400 cycles is calculated and shown in Fig. 5b. The average CE for the initial 400 cycles under a current density-plating capacity pairing of 2 mA cm^{-2} - 2 mAh cm^{-2} , 3 mA cm^{-2} - 3 mAh cm^{-2} , and

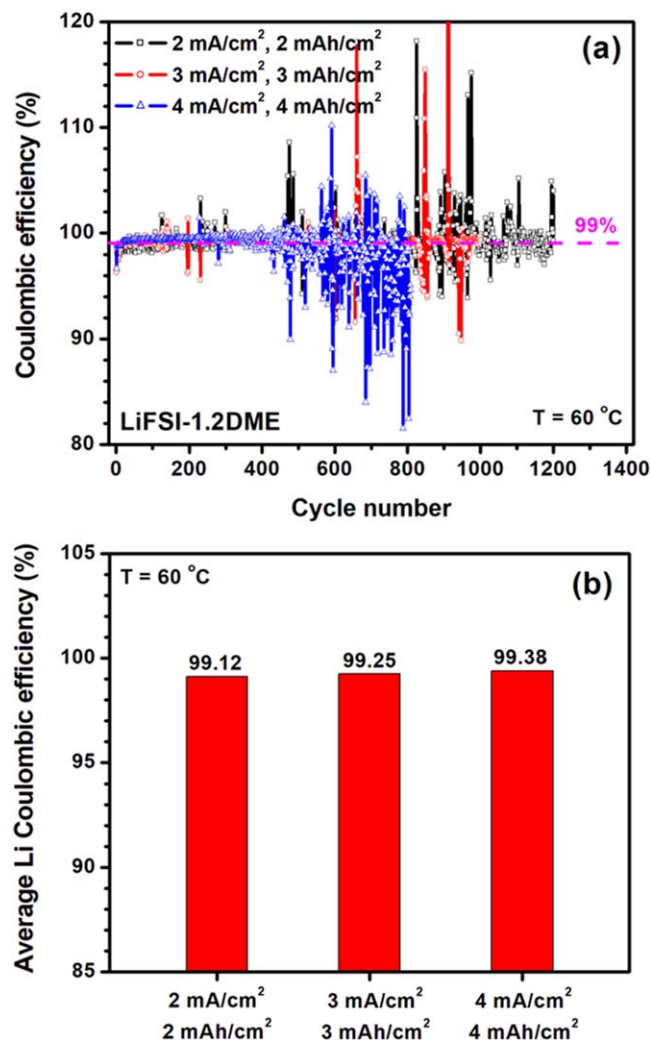


Figure 5. (a) Stability of Li Coulombic efficiency with cycling, and (b) average Li Coulombic efficiency during the initial 400 cycles measured in Li || Cu cells under different plating/stripping current densities (2, 3, and 4 mA cm⁻²) and plating capacities (2, 3, and 4 mAh cm⁻²) with a highly concentrated LiFSI-1.2DME electrolyte.

4 mA cm⁻²–4 mAh cm⁻² at 60 °C is 99.12, 99.25 and 99.38%, respectively. Such a high average CE is seldom reported in the literature.^{35,46} This result is encouraging for achieving long-lasting (500–1000 cycles) LMBs with NMC622 cathodes with a high areal capacity (e.g. 3–4 mAh cm⁻²) under high C-rate (e.g. 1C). Moreover, the average CE surprisingly increases with increasing plating capacity, a phenomenon that was also reported by Adams et al.⁴⁶ The authors attributed it to a better stabilization of the SEI or passivation layer in the early stages of cycling using a higher plating capacity.⁴⁶ However, after 400 cycles, the CE becomes more unstable, especially for the case under a very high current density of 4 mA cm⁻² and a very high plating capacity of 4mAh cm⁻². For a Li metal anode with a similar Li CE, the absolute amount of loss of Li per cycle increases with increasing Li plating capacity, which means the SEI layer grown on the surface of Li metal anode becomes thicker during each cycle when a higher plating capacity is applied. After 400 cycles, the continuously growing SEI layer becomes much thicker in the case of a higher plating capacity. This extremely thick SEI may be more prone to break up due to large volume change under a high plating capacity, leading to the instability of Li CE.

Figure 6a shows the voltage profiles of Li plating and stripping during the 5th cycle for Li (250 μm thick) || Cu cells in LiFSI-1.2DME electrolytes without and with 1 wt.% TAP at various

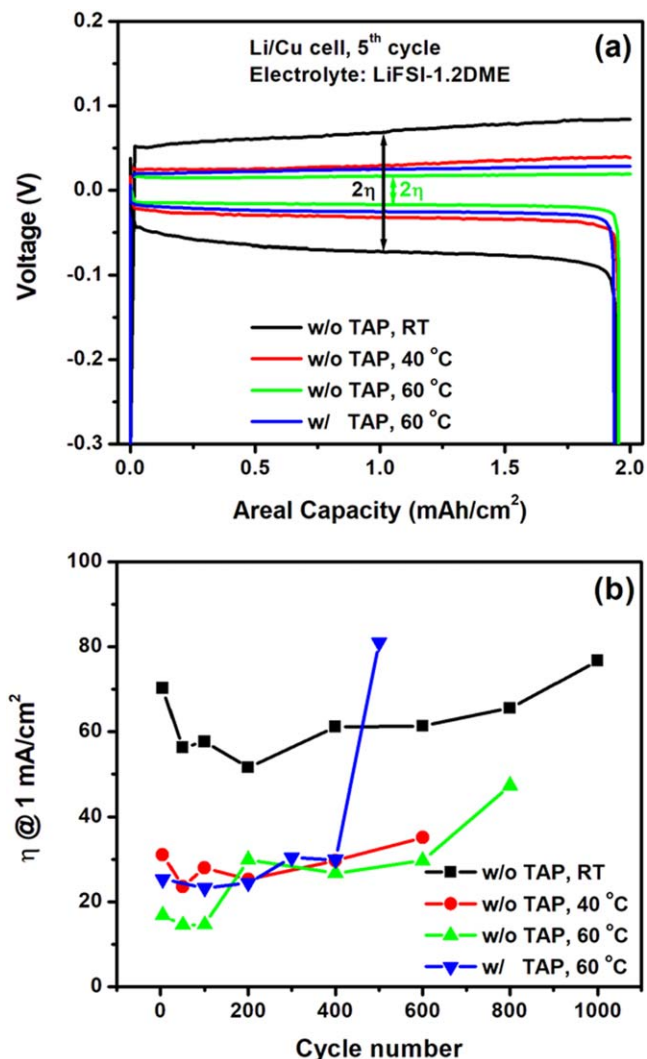


Figure 6. (a) Voltage profiles of the 5th Li plating/stripping cycle, and (b) overpotential (η) related to Li plating/stripping process as a function of cycle number for Li (250 μm thick) || Cu cells in LiFSI-1.2DME without and with 1 wt.% TAP electrolytes at various temperatures (room temperature (RT), 40 °C and 60 °C). The plating/stripping current density and plating capacity during cycling is 1 mA cm⁻² and 2 mAh cm⁻², respectively.

temperatures (RT, 40 °C and 60 °C). The plating/stripping current density and total plating capacity during cycling is 1 mA cm⁻² and 2 mAh cm⁻², respectively. During the plating step, Li is stripped from the Li foil and then plated onto the Cu substrate; while during the stripping step, the deposited Li is stripped from the Cu substrate and plated back onto the Li foil. Therefore, the voltage profile for the plating step should be symmetric with that of the stripping step, and the overpotential (η) during both processes should be approximately the same. Thus, the overpotential can be extracted as half of the difference between the plating and stripping voltage profiles, as labeled in Fig. 6a. In the case of the pure LiFSI-1.2DME electrolyte, the overpotential related to Li plating/stripping decreases with increasing operating temperature. For example, the overpotential located at a plating/stripping capacity of 1 mAh cm⁻² is ~70.2, ~30.1 and ~16.8 mV at RT, 40 °C and 60 °C, respectively. This means that the portion of the Li || NMC622 full cell overpotential attributed to the Li plating/stripping process during charging/discharging, respectively, becomes small at an elevated temperature. Such low overpotential at the interfaces between Li metal anodes and HCEs is beneficial for enhancing the rate capability of LMBs. When 1 wt.% TAP is added into LiFSI-1.2DME electrolyte, the

overpotential at a plating/stripping capacity of 1 mAh cm^{-2} and a temperature of 60°C increases slightly from $\sim 16.8 \text{ mV}$ for pure LiFSI-1.2DME to $\sim 25.3 \text{ mV}$.

In order to investigate the cycle stability of the Li plating/stripping process, the overpotential (η) for the Li plating/stripping process for a plating/stripping capacity of 1 mAh cm^{-2} is extracted from the voltage profiles of the Li ($250 \mu\text{m}$ thick) || Cu cells as a function of cycle number (Figs. S2 and S3). The results are shown in Fig. 6b for the Li || Cu cells in LiFSI-1.2DME without and with 1 wt.% TAP electrolytes at various temperatures (RT, 40°C and 60°C). In the case of pure LiFSI-1.2DME electrolyte, for all three temperatures, the overpotential initially decreases with cycling due to an activation process, and then gradually increases with cycling. In the case of LiFSI-1.2DME with 1 wt.% TAP at 60°C , there is some slight variation in the overpotential during the initial 400 cycles; while there is a sudden jump in the overpotential after 500 cycles, which may be due to the poor contact between cell components. It is important to note that for the case of pure LiFSI-1.2DME, the overpotentials of both fresh and aged cells at 60°C are still smaller than that at RT for all cycle numbers. It is thus clear that Li metal anodes can be stably cycled at 60°C under a current density of 1 mA cm^{-2} for at least 400 cycles while maintaining a small overpotential of $< 31 \text{ mV}$ in the cases of both the pure electrolyte and the electrolyte with 1 wt.% TAP. A stable Li metal anode with a small overpotential (Fig. 6b) together with high Li CE (Figs. 4 and 5) is a key to achieving stable LMBs under relatively high C-rate (such as C/3 rate charge and 1C discharge) in HCEs at elevated temperatures.

Effect of temperature on cycling test of Li || NMC622 coin cells.—Figure 7 shows the cycling performance of Li || NMC622 coin cells with $250 \mu\text{m}$ thick Li chips in the two HCEs considered in this study without TAP at both RT and 60°C . The cells were cycled between 2.8 and 4.3 V under C/3-C/3 charge-discharge at RT and C/3-1C charge-discharge at 60°C . In the case of LiFSI-2.4DME electrolyte at RT, the discharge capacity gradually decreases with cycle number within 150 cycles followed by a rapid drop over the

next ~ 40 cycles. At RT, the C/3 capacity retention of the cell with the LiFSI-2.4DME electrolyte drops to 80% at 160 cycles, and the cell CE is quite stable within 189 cycles with an average CE as high as $\sim 99.57\%$. By increasing LiFSI/DME molar ratio from 1/2.4 to 1/1.2 (i.e. from LiFSI-2.4DME to LiFSI-1.2DME), a significant increase in the stability of the cycling performance is achieved. At RT, the cell in the LiFSI-1.2DME electrolyte can achieve ~ 301 cycles at a C/3 capacity retention of 80%, which is almost double the ~ 160 cycles achieved by the cell with the LiFSI-2.4DME electrolyte at the same capacity retention. Moreover, in the case of LiFSI-1.2DME electrolyte at RT, the cell CE is quite stable for 379 cycles with an average CE as high as $\sim 99.83\%$, which is higher than that in the case of the LiFSI-2.4DME electrolyte at the same temperature. These results far surpass those of a conventional dilute liquid electrolyte such as 1 M LiPF_6 in EC/EMC + 2% VC (Fig. S4).

Given the presence of both a thick lithium anode ($250 \mu\text{m}$) and its cathode counterpart in these full cells, it is important to delineate the sources of capacity fade. During the charge step, Li is extracted from NMC622 cathodes and then electroplated onto Li metal anodes. Due to the side reactions of Li metal with the electrolyte (i.e. SEI formation/growth), some of the Li from the cathode is lost. Since a Li metal anode with much higher capacity than that of an NMC622 cathode provides an excess Li source, Li with an equivalent capacity to that of the previous charge step can be stripped from the Li metal anode and moved back to NMC622 cathodes. Therefore, the cell Coulombic inefficiency (i.e. $100\% - \text{CE}$) during cycling is actually attributed to the side reactions at the NMC cathodes (e.g. the decomposition of the electrolyte) and the degradation of NMC cathodes (e.g. loss of active mass). As shown in Fig. 7, the LiFSI-2.4DME electrolyte can be used for LMBs with high voltage NMC cathodes for more than 189 stable cycles at RT, a significant improvement over the results from studies using similar electrolytes reported in the literature. Generally, ether solvents such as DME are believed to be unstable at high voltages of $> 4.0 \text{ V}$ (vs Li/Li⁺). For example, Fan et al.²⁸ reported that their Li || NMC622 cell using 4 M LiFSI/DME electrolyte failed during the first cycle charge when the charge voltage was above 4.15 V and attributed it to the continuous

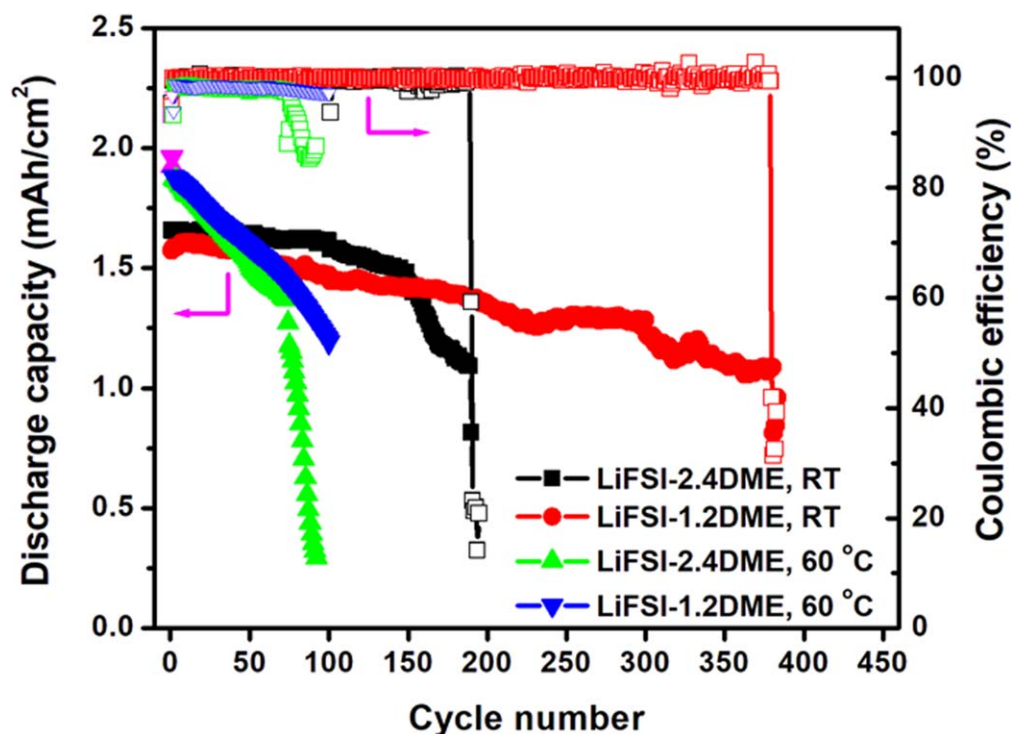


Figure 7. Cycling performance of Li ($250 \mu\text{m}$ thick) || NMC622 in two types of LiFSI/DME electrolytes with different salt/solvent molar ratios: LiFSI-2.4DME and LiFSI-1.2DME. The magenta spike data points are for C/10 charge and C/10 discharge for the fresh cells. The cycling condition was as follows: C/3 charge and C/3 discharge at room temperature (RT) and C/3 charge and 1C discharge at 60°C .

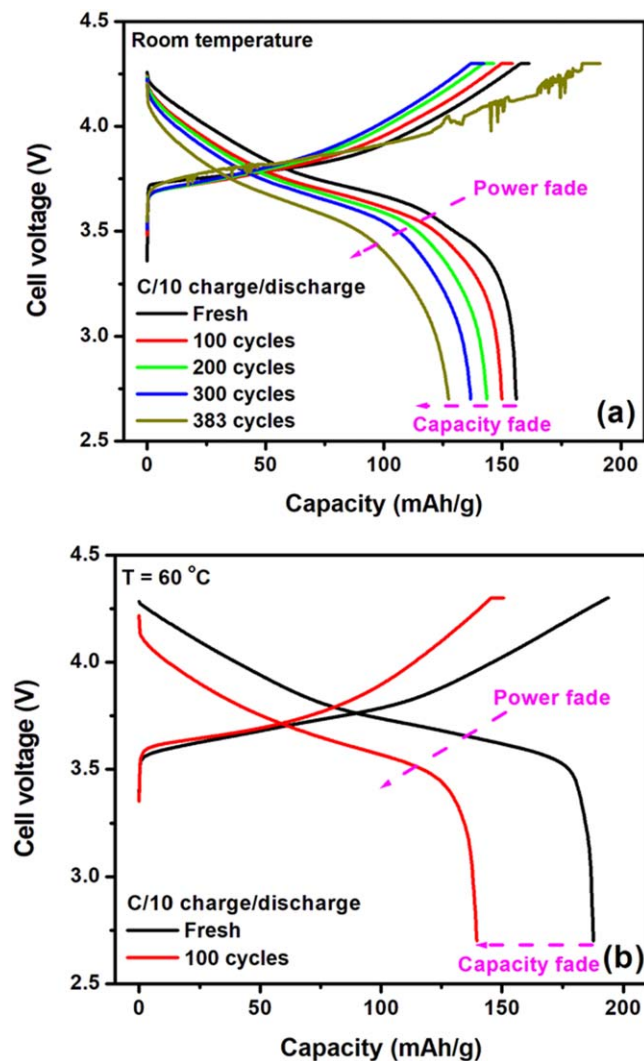


Figure 8. C/10 charge/discharge voltage profiles of fresh and aged Li (250 μm thick) || NMC622 cells in the LiFSI-1.2DME electrolytes at (a) room temperature and (b) 60 $^{\circ}\text{C}$.

oxidation of DME solvents. In this work, the Li || NMC622 coin cell with LiFSI-2.4DME electrolyte achieved more than 189 stable cycles between 2.8–4.3 V at RT. This may be due to the use of LiFSI salts of high purity with a small amount (≤ 20 ppm) of chloride in the present work. Han et al.⁴⁷ reported that the passivation of Al can be achieved at 4.2 V vs Li⁺/Li by liquid carbonate electrolytes made from highly pure LiFSI (with Cl⁻ < 1 ppm) while Al corrosion can occur when the LiFSI based electrolyte contains ~ 50 ppm Cl⁻. Additionally, Jung et al.^{48,49} investigated the cycling stability of Ni-rich NMC cathode materials and found that at high voltages, Ni-rich NMC such as NMC622 can release very reactive lattice oxygen, which promotes the oxidation of carbonate electrolytes (e.g. ethylene carbonate (EC)) on the surface of NMC cathode materials. Similarly, in this work DME can be oxidized via the reaction between released lattice oxygen and DME on the surface of the NMC622 cathode. The reaction rate depends on the product of the concentration of lattice oxygen on the surface of NMC cathode materials and the concentration of free DME. By increasing the LiFSI/DME molar ratio (from LiFSI-2.4DME to LiFSI-1.2DME), the concentration of free DME in the HCE decreases, thus reducing the side reaction rate and increasing the stability of the electrolyte, which increases the cell CE and thus enhances the cycle stability of the Li || NMC622 cells at RT.

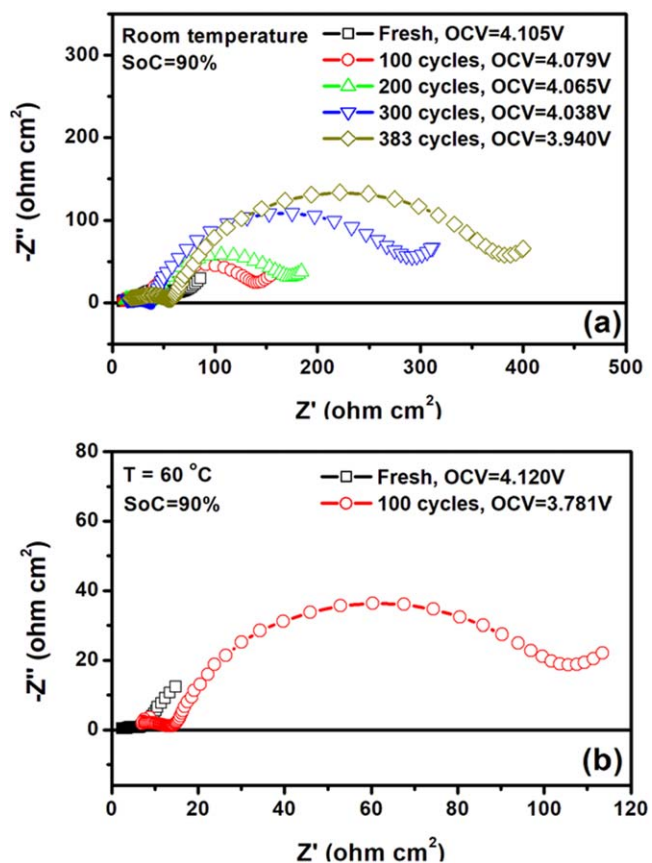


Figure 9. Nyquist plots of Li (250 μm thick) || NMC622 cells as a function of cycle number in the LiFSI-1.2DME electrolytes at (a) room temperature and (b) 60 $^{\circ}\text{C}$.

When the operating temperature is elevated to 60 $^{\circ}\text{C}$, the cycling stability of the Li || NMC622 cells becomes worse in both LiFSI-2.4DME and LiFSI-1.2DME electrolytes. For example, the cycle life of the cells with the LiFSI-2.4DME and LiFSI-1.2DME electrolyte is only 51 and 64 cycles at a 1C capacity retention of 80% at 60 $^{\circ}\text{C}$, respectively, which is much shorter than that of the cells with corresponding electrolytes at RT (i.e. ~ 160 and ~ 301 cycles at a C/3 capacity retention of 80% for LiFSI-2.4DME and LiFSI-1.2DME electrolytes, respectively). Moreover, the average cell CE decreases with increasing temperature. In the case of the LiFSI-2.4DME electrolyte at 60 $^{\circ}\text{C}$, the cell CE is stable for only 73 cycles with an average CE of $\sim 97.87\%$; and in the case of LiFSI-1.2DME electrolyte at 60 $^{\circ}\text{C}$, the cell CE is stable for only 100 cycles with an average CE of $\sim 98.21\%$. The average cell CE in both cases at 60 $^{\circ}\text{C}$ is much lower than that at RT (i.e. ~ 99.57 and $\sim 99.83\%$ for LiFSI-2.4DME and LiFSI-1.2DME electrolytes, respectively). The shorter cycle life and lower cell CE is due to the increased severity of the side reactions at the cathode at elevated temperatures. Jung et al.⁴⁹ investigated the temperature dependence of oxygen release from NMC622 cathodes caused by the transformation of the near-surface structure from layered to spinel and/or rock-salt structure and found that the onset potential for oxygen release in NMC-graphite cells decreases and the rate of oxygen release increases with increasing temperature. In this work, at elevated temperatures, the higher rate of oxygen releases leads to the accelerated degradation of NMC cathode and promotes more severe side reaction between lattice oxygen and DME on the surface of the NMC622 cathode materials. These results demonstrate the cycling stability of LMBs utilizing the LiFSI-2.4DME and LiFSI-1.2DME electrolytes at RT; however, such stability deteriorates at 60 $^{\circ}\text{C}$. This represents a dilemma when considering battery operation at elevated temperatures is required for

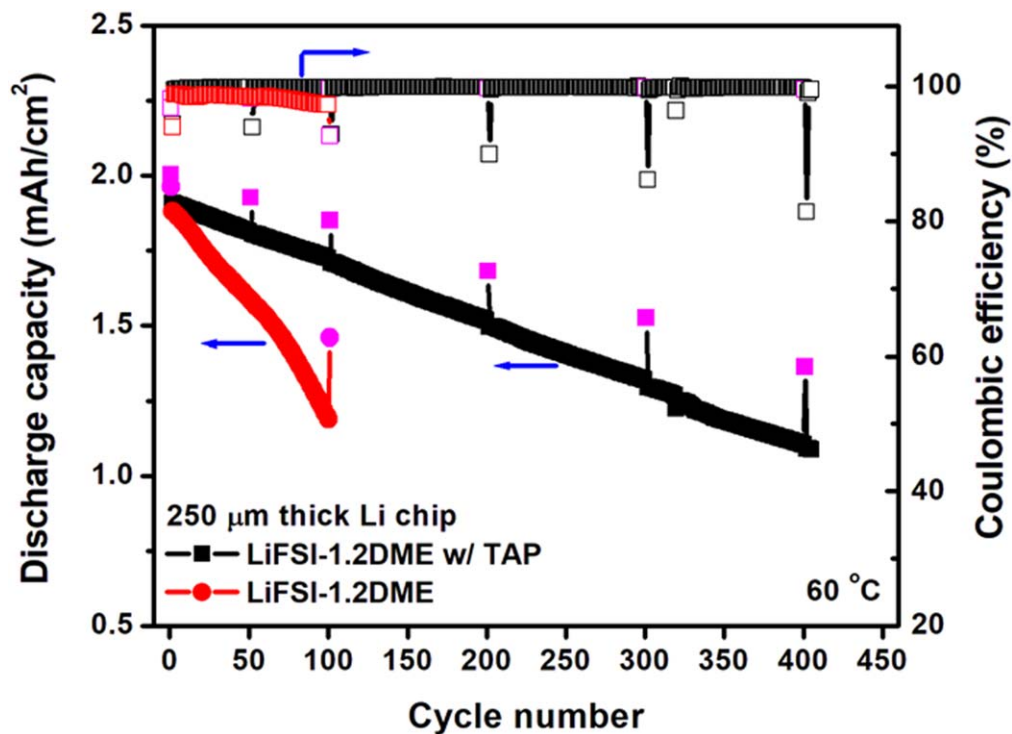


Figure 10. Cycling performance of Li (250 μm thick) || NMC622 cells in the LiFSI-1.2DME electrolytes with 1 wt.% TAP additive at 60 $^{\circ}\text{C}$. The cycling condition was C/3 charge and 1C discharge. The magenta spike data points are for C/10 charge and C/10 discharge during reference performance tests. For a comparison, the cycling performance of the Li (250 μm thick) || NMC622 cell under the same operating condition in the pure LiFSI-1.2DME is also plotted.

acceptable rate capability, as mentioned earlier. Thus, the LiFSI-2.4DME and LiFSI-1.2DME electrolytes alone are not suitable for LMBs with a relatively good cycle life at elevated temperatures.

Figure 8 shows the C/10 charge/discharge voltage profiles of fresh and aged Li (250 μm thick) || NMC622 cells in the LiFSI-1.2DME electrolytes at RT and 60 $^{\circ}\text{C}$. In the case of LiFSI-1.2DME electrolyte, at RT, C/10 capacity retention is 87.8% and 81.8% at 300 and 383 cycles, respectively. In addition to capacity fade, power fade during cycling is observed even for C/10 charge/discharge testing. Based on the average Li CE of $\sim 99.0\%$ (Fig. 4) and total accumulated discharge capacity of $\sim 514 \text{ mAh cm}^{-2}$ during cycling test for 379 stable cycles (Fig. 7), the areal capacity of Li consumed is calculated to be only $\sim 5.14 \text{ mAh cm}^{-2}$, which is $\sim 10.0\%$ of the total areal capacity ($\sim 51.5 \text{ mAh cm}^{-2}$) of Li metal anode with a thickness of 250 μm . This means even after 379 cycles, there is still excess Li available at the anode. Therefore, the C/10 capacity fade is due to the capacity loss of the NMC622 cathode and the power fade is due to the increase in cell resistance. When the operating temperature is increased to 60 $^{\circ}\text{C}$, the cell degrades very quickly. The C/10 capacity retention is only $\sim 80.3\%$ after 100 cycles. In addition, severe power fade is observed even under C/10 charge/discharge (Fig. 8b), a result of the significant increase in the cell resistance after aging for 100 cycles at 60 $^{\circ}\text{C}$.

Figure 9 shows the impedance plots of Li (250 μm thick) || NMC622 cells as a function of cycle number in the LiFSI-1.2DME electrolytes at RT and 60 $^{\circ}\text{C}$. It is found that the cell resistance significantly increased with cycling. At RT, the total cell resistance (excluding mass transport resistance) increased from $\sim 62 \text{ ohm cm}^2$ for the fresh cell to $\sim 300 \text{ ohm cm}^2$ for the cell aged for 300 cycles. The significant increase of cell resistance is caused by the growth of surface film on NMC622 cathode,⁵⁰ the increase in charge transfer resistance,⁵⁰ and the SEI layer formation/growth on the Li metal anode. The evolution of cell resistance with cycling leads to more severe capacity fade under C/3 charge/discharge than under C/10 at the same cycle. For example, after 300 cycles, the C/3 capacity retention is only $\sim 81.6\%$ (Fig. 7), which is lower than the C/10

capacity retention of $\sim 87.8\%$ (Fig. 8a). With the increase of operating temperature from RT to 60 $^{\circ}\text{C}$, the cell resistance increases at a much higher rate. For example, the cell resistance increases by almost an order of magnitude over that of the fresh cell after only 100 cycles at 60 $^{\circ}\text{C}$. The acceleration of the cell resistance growth at elevated temperature is due to the increased instability of the electrolyte.

Cycling test of Li || NMC622 coin cells at elevated temperature.—In order to extend the cycle life of Li || NMC622 coin cells at elevated temperatures, 1 wt.% TAP was added into the LiFSI-1.2DME electrolyte. TAP has been reported as an electrolyte additive capable of increasing the stability of Li-ion batteries with graphite anodes and NMC cathodes at high voltage and high temperature conditions.^{42,43} Figure 10 shows cycling performance of Li || NMC622 coin cells with 250 μm thick Li anodes in LiFSI-1.2DME with 1 wt.% TAP at 60 $^{\circ}\text{C}$. The cycling condition is C/3 charge and 1C discharge between 2.8 and 4.3 V. For a comparison, the cycling performance of Li (250 μm thick) || NMC622 cell in the pure LiFSI-1.2DME under the same operating conditions is also plotted. In the case of the electrolyte with 1 wt.% TAP at 60 $^{\circ}\text{C}$, the cell achieved ~ 194 and ~ 291 cycles at a 1C capacity retention of 80% and 70%, respectively, which is much higher than that in the case of pure electrolyte at the same temperature. Moreover, the addition of TAP increases the cell CE at elevated temperatures. In the case of the electrolyte with 1 wt.% TAP, the cell CE is stable for more than 400 cycles with an average CE of 99.74% (excluding the first cycle of resumed test) at 60 $^{\circ}\text{C}$, which is much better than that (i.e. $\sim 98.21\%$) of the pure electrolyte case at the same temperature. Figure 11 shows the C/10 charge/discharge voltage profiles and impedance plots of fresh and aged Li (250 μm thick) || NMC622 cells in the LiFSI-1.2DME electrolyte with 1 wt.% TAP additive at 60 $^{\circ}\text{C}$. Compared to the case of pure LiFSI-DME electrolyte (Fig. 8b), the degradation of the cell becomes slow with the addition of TAP. In the case of the electrolyte with 1 wt.% TAP, the C/10 capacity retention is $\sim 84.0\%$ and 68.1% after cycling for 200 and 400 cycles, respectively, which is much better than that in the case of

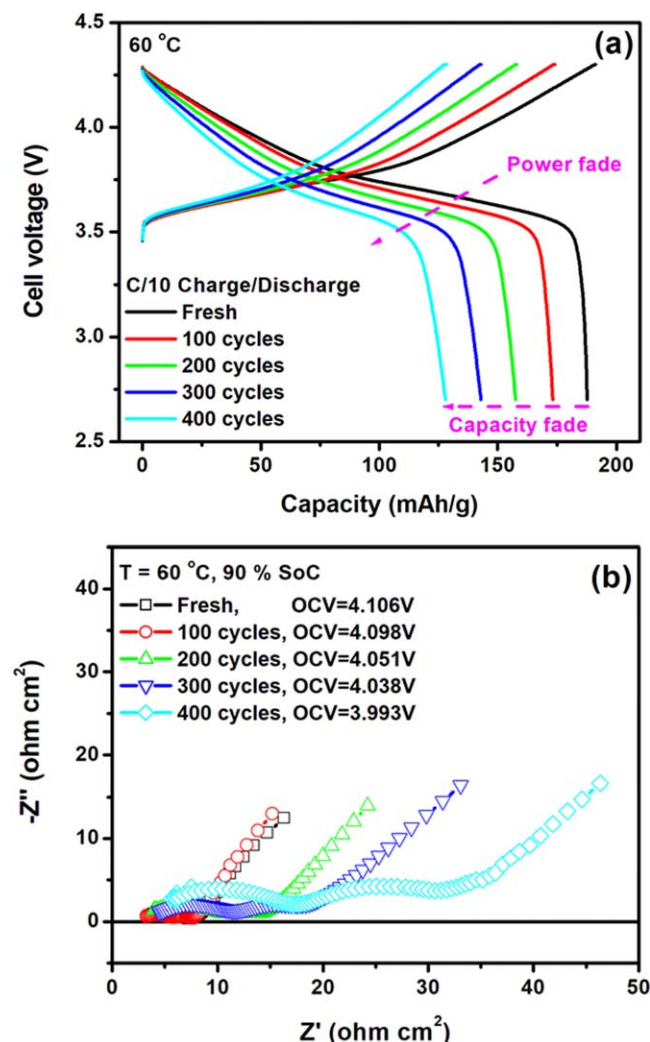


Figure 11. (a) C/10 charge/discharge voltage profiles and (b) Nyquist plots of fresh and aged Li || NMC622 cells with a 250 μm Li chip at 60 °C in the LiFSI-1.2DME electrolyte with 1 wt.% TAP additive.

pure electrolyte. Besides the capacity fade, some power fade is observed in the electrolyte with TAP, albeit minimal compared to the corresponding pure electrolyte case. This is consistent with the slower rate of cell resistance increase for the cell containing TAP illustrated in Fig. 11b as compared to the pure electrolyte results in Fig. 9b. Specifically, the total resistance of the cell in the electrolyte with 1 wt.% TAP increases from ~ 7.2 ohm cm^2 for the fresh cell to ~ 19 and ~ 32 ohm cm^2 for the cells after being cycled for 300 and 400 cycles, respectively, which is still much smaller than that (~ 105 ohm cm^2) of the cell with the pure electrolyte after being cycled for only 100 cycles. Xia et al.⁴³ reported that TAP can form a thick and dense interfacial film at the surfaces of both graphite and NMC electrodes via the polymerization of triallyl phosphate molecules. Our recent work also confirms this finding.⁴² In this work, the thick and dense film formed from TAP on the surface of NMC622 cathode materials reduces the rate of lattice oxygen release and improves the stability of NMC622 cathode materials. This, in turn, limits the reaction of DME in the electrolyte with lattice oxygen on the surface of NMC622 cathode materials, simultaneously enhancing the stability of the electrolyte. This significantly extends the cycle life and slows the impedance rise of the Li || NMC622 coin cells in the HCE electrolyte with 1 wt.% TAP as compared to that of the pure electrolyte cells at elevated temperatures.

In the literature, LMBs reported often adopt very thick (≥ 250 μm) Li anodes containing more than an order of magnitude

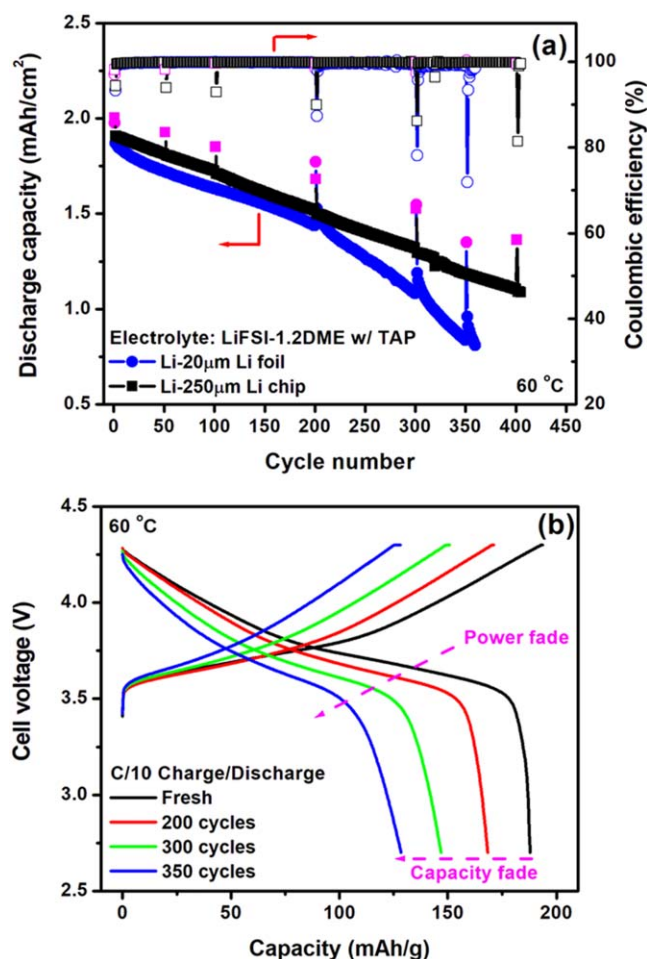


Figure 12. (a) Cycling performance of Li (20 μm thick) || NMC622 cells, and (b) C/10 charge/discharge voltage profiles of fresh and aged cells at 60 °C in the LiFSI-1.2DME electrolyte with 1 wt.% TAP additive. The cycling condition was C/3 charge and 1C discharge. The magenta spike data points are for C/10 charge and C/10 discharge during reference performance tests. For a comparison, the cycling performance of the Li (250 μm thick) || NMC622 cell under the same operating condition in the same electrolyte was also plotted in (a).

of Li greater than the amount actually being cycled, which significantly reduces the energy density of LMBs.^{6,45,51} For example, if the ratio of negative (Li) electrode to positive electrode (NMC622) capacity (N/P ratio) is more than 10, the practical specific capacity of Li metal anodes is less than 386 mAh g^{-1} , which is close to that of graphite anodes in conventional Li-ion batteries. Therefore, such LMBs cannot be implemented for practical use since they cannot achieve an acceptable increase in practical energy density over state-of-the-art Li-ion batteries with graphite anodes and the same cathodes. Moreover, this huge Li excess could make the interpretation of the results on cycling stability of LMBs more difficult.⁵¹ As discussed previously, the Li anode with a huge Li excess can provide an almost infinite Li source to replenish the Li loss due to SEI formation/growth (i.e. Li Coulombic inefficiency) during cycling. Thus, the cell cycle life depends on the cathode stability rather than the cycling stability of Li metal anodes, artificially enhancing the cycling stability of LMBs. Therefore, it is desirable to limit the excess Li when evaluating the cycling stability of LMBs utilizing the newly developed electrolytes presented in this work.

Figure 12a shows the cycling performance of a Li || NMC622 coin cell with 20 μm thick Li foil in the LiFSI-1.2DME electrolyte with 1 wt.% TAP at 60 °C. The cycling condition is C/3 charge and 1C discharge between 2.8 and 4.3 V. The cycling performance of the

Li (250 μm thick) || NMC622 cell in the same electrolyte under the same operating conditions is also plotted for a comparison. For Li || NMC622 coin cells with 20 μm thick Li foil, the ratio of negative (Li) to positive electrode (NMC622) capacity (N/P ratio) is only ~ 2.1 . A 2Ah-format pouch cell designed based on the same cell components as the coin cell is expected to have an energy density as high as $\sim 250 \text{ Wh kg}^{-1}$ (Table S1), which is much higher than that of Li-ion batteries with the same NMC622 cathodes and corresponding graphite anodes. Figure 12a shows that even after reducing the Li foil thickness to 20 μm , the cell can achieve ~ 175 and ~ 240 cycles at a 1C capacity retention of 80% and 70% at 60 $^{\circ}\text{C}$, respectively. This results from the high Li CE ($\geq 98.8\%$) of the Li metal anode in the newly developed HCE and the enhanced overall cycling stability of the cell achieved through the addition of TAP to the HCE at elevated temperatures. Moreover, for ~ 200 cycles, the cell with 20 μm thick Li foil follows a similar degradation trend to that of the cell with the 250 μm Li chip. Except for the difference in the Li anode thickness, both cells are the same, including the Li-electrolyte and NMC-electrolyte interfacial reactions. Therefore, it is not surprising that the degradation behavior of both cells is similar before Li is nearly fully consumed. The average cell CE for the initial 200 cycles is calculated to be $\sim 99.76\%$ for the cell with 20 μm thick Li foil, which is close to $\sim 99.71\%$ for the cell with 250 μm thick Li chip. Figure 12b shows the C/10 charge/discharge voltage profiles of the fresh and aged Li (20 μm thick) || NMC622 cell in the LiFSI-1.2DME electrolyte with 1 wt.% TAP at 60 $^{\circ}\text{C}$. In the case of the cell with 20 μm thick Li foil, the C/10 capacity retention is $\sim 89.7\%$ and $\sim 78.2\%$ after cycling for 200 and 300 cycles, respectively, which is close to that ($\sim 84.0\%$ and 76.1% after cycling for 200 and 300 cycles) of the cell with the 250 μm thick Li chip. These results demonstrate that the newly developed LiFSI-1.2DME electrolyte with 1 wt.% TAP can enable stable LMBs with high voltage NMC622 cathodes and limited Li excess at elevated temperatures.

Conclusions

The temperature effect on the performance of LMBs, the Li Coulombic efficiency, and the cycle stability in highly concentrated LiFSI-DME electrolytes with different salt/solvent molar ratios was investigated. High energy density and enhanced rate capability in LMBs with NMC622 cathodes at elevated temperatures are observed. Additionally, at 60 $^{\circ}\text{C}$, the Li Coulombic efficiency remains almost constant in the highly concentrated LiFSI-DME electrolytes with salt/solvent molar ratios of both 1/2.4 and 1/1.2. A higher salt/solvent molar ratio is shown to provide an enhancement in the cycling stability of LMBs with NMC622 cathodes at RT, but these pure electrolytes are shown to be ineffective at elevated temperatures by way of rapid capacity fade and low CE. Introduction of TAP as an electrolyte additive in the highly concentrated LiFSI-DME electrolyte not only yields a sustained Li Coulombic efficiency as high as $\sim 98.8\%$, but also significantly enhances the cycling ability of LMBs with NMC622 cathode at elevated temperatures. Thus, the combination of a high salt/solvent molar ratio together with addition of TAP in an electrolyte can enable ether-based electrolytes for stable, high energy density LMBs with high voltage NMC622 cathodes at elevated temperatures.

ORCID

Yongjun Leng  <https://orcid.org/0000-0001-9868-0195>
 Ryan S. Longchamps  <https://orcid.org/0000-0002-8168-8032>
 Chao-Yang Wang  <https://orcid.org/0000-0003-0650-0025>

References

- X.-G. Yang, T. Liu, Y. Gao, S. Ge, Y. Leng, D. Wang, and C.-Y. Wang, *Joule*, **3**, 3002 (2019).
- Z. A. Needell, J. McNerney, M. T. Chang, and J. E. Trancik, *Nat. Energy*, **1**, 16112 (2016).
- Z. P. Cano, D. Banham, S. Y. Ye, A. Hintennach, J. Lu, M. Fowler, and Z. W. Chen, *Nat. Energy*, **3**, 279 (2018).

- Y. Guo, H. Li, and T. Zhai, *Adv. Mater.*, **29**, 1700007 (2017).
- B. Liu, J.-G. Zhang, and W. Xu, *Joule*, **2**, 833 (2018).
- J. Liu, Z. Bao, Y. Cui, E. J. Dufek, J. B. Goodenough, P. Khalifah, Q. Li, B. Y. Liaw, P. Liu, A. Manthiram, Y. S. Meng, V. R. Subramanian, M. F. Toney, V. V. Viswanathan, M. S. Whittingham, J. Xiao, W. Xu, J. Yang, X.-Q. Yang, and J.-G. Zhang, *Nat. Energy*, **4**, 180 (2019).
- Y. Liu, D. Lin, Z. Liang, J. Zhao, K. Yan, and Y. Cui, *Nat. Commun.*, **7**, 10992 (2016).
- Y. Sun, G. Zheng, Z. W. Seh, N. Liu, S. Wang, J. Sun, H. R. Lee, and Y. Cui, *Chem*, **1**, 287 (2016).
- K. Liu, A. Pei, H. R. Lee, B. Kong, N. Liu, D. Lin, Y. Liu, C. Liu, P. C. Hsu, Z. Bao, and Y. Cui, *Journal of the American Chemical Society*, **139**, 4815 (2017).
- Y. Gao, M. Guo, K. Yuan, C. Shen, Z. Ren, K. Zhang, H. Zhao, F. Qiao, J. Gu, Y. Qi, K. Xie, and B. Wei, *Adv. Energy Mater.*, **10**, 1903362 (2019).
- D. Lee, S. Sun, J. Kwon, H. Park, M. Jang, E. Park, B. Son, Y. Jung, T. Song, and U. Paik, *Adv. Mater.*, **32**, 1905573 (2020).
- L. Liu, Y. X. Yin, J. Y. Li, S. H. Wang, Y. G. Guo, and L. J. Wan, *Adv. Mater.*, **30**, 1706216 (2018).
- C. Yang, L. Zhang, B. Liu, S. Xu, T. Hamann, D. McOwen, J. Dai, W. Luo, Y. Gong, E. D. Wachsman, and L. Hu, *PNAS*, **115**, 3770 (2018).
- C. P. Yang, Y. X. Yin, S. F. Zhang, N. W. Li, and Y. G. Guo, *Nat. Commun.*, **6**, 8058 (2015).
- T. T. Zuo, X. W. Wu, C. P. Yang, Y. X. Yin, H. Ye, N. W. Li, and Y. G. Guo, *Adv. Mater.*, **29**, 1700389 (2017).
- X. Liang, Q. Pang, I. R. Kocchetkov, M. S. Sempere, H. Huang, X. Sun, and L. F. Nazar, *Nat. Energy*, **2**, 17119 (2017).
- Z. Tu, S. Choudhury, M. J. Zachman, S. Wei, K. Zhang, L. F. Kourkoutis, and L. A. Archer, *Nat. Energy*, **3**, 310 (2018).
- M. Wan, S. Kang, L. Wang, H. W. Lee, G. W. Zheng, Y. Cui, and Y. Sun, *Nat. Commun.*, **11**, 829 (2020).
- Y. Gao, Z. Yan, J. L. Gray, X. He, D. Wang, T. Chen, Q. Huang, Y. C. Li, H. Wang, S. H. Kim, T. E. Mallouk, and D. Wang, *Nat. Mater.*, **18**, 384 (2019).
- N. W. Li, Y. X. Yin, C. P. Yang, and Y. G. Guo, *Adv. Mater.*, **28**, 1853 (2016).
- X.-B. Cheng, C. Yan, X. Chen, C. Guan, J.-Q. Huang, H.-J. Peng, R. Zhang, S.-T. Yang, and Q. Zhang, *Chem*, **2**, 258 (2017).
- G. Li, Q. Huang, X. He, Y. Gao, D. Wang, S. H. Kim, and D. Wang, *ACS Nano*, **12**, 1500 (2018).
- R. Xu, X.-B. Cheng, C. Yan, X.-Q. Zhang, Y. Xiao, C.-Z. Zhao, J.-Q. Huang, and Q. Zhang, *Mater*, **1**, 317 (2019).
- X. Li, J. Zheng, X. Ren, M. H. Engelhard, W. Zhao, Q. Li, J.-G. Zhang, and W. Xu, *Adv. Energy Mater.*, **8**, 1703022 (2018).
- E. Markevich, G. Salitra, F. Chesneau, M. Schmidt, and D. Aurbach, *ACS Energy Lett.*, **2**, 1321 (2017).
- R. Miao, J. Yang, Z. Xu, J. Wang, Y. Nuli, and L. Sun, *Sci. Rep.*, **6**, 21771 (2016).
- J. Wang, Y. Yamada, K. Sodeyama, C. H. Chiang, Y. Tateyama, and A. Yamada, *Nat. Commun.*, **7**, 12032 (2016).
- X. Fan, L. Chen, X. Ji, T. Deng, S. Hou, J. Chen, J. Zheng, F. Wang, J. Jiang, K. Xu, and C. Wang, *Chem*, **4**, 174 (2018).
- J. Qian, W. A. Henderson, W. Xu, P. Bhattacharya, M. Engelhard, O. Borodin, and J. G. Zhang, *Nat. Commun.*, **6**, 6362 (2015).
- L. Suo, Y. S. Hu, H. Li, M. Armand, and L. Chen, *Nat. Commun.*, **4**, 1481 (2013).
- L. M. Suo, W. J. Xue, M. Gobet, S. G. Greenbaum, C. Wang, Y. M. Chen, W. L. Yang, Y. X. Li, and J. Li, *PNAS*, **115**, 1156 (2018).
- Y. Yamada, J. Wang, S. Ko, E. Watanabe, and A. Yamada, *Nat. Energy*, **4**, 269 (2019).
- X. Ren, L. Zou, S. Jiao, D. Mei, M. H. Engelhard, Q. Li, H. Lee, C. Niu, B. D. Adams, C. Wang, J. Liu, J.-G. Zhang, and W. Xu, *ACS Energy Lett.*, **4**, 896 (2019).
- X. Ren, L. Zou, X. Cao, M. H. Engelhard, W. Liu, S. D. Burton, H. Lee, C. Niu, B. E. Matthews, Z. Zhu, C. Wang, B. W. Arey, J. Xiao, J. Liu, J.-G. Zhang, and W. Xu, *Joule*, **3**, 1662 (2019).
- S. Chen, J. Zheng, D. Mei, K. S. Han, M. H. Engelhard, W. Zhao, W. Xu, J. Liu, and J. G. Zhang, *Adv. Mater.*, **30**, 1706102 (2018).
- X. Ren, S. Chen, H. Lee, D. Mei, M. H. Engelhard, S. D. Burton, W. Zhao, J. Zheng, Q. Li, M. S. Ding, M. Schroeder, J. Alvarado, K. Xu, Y. S. Meng, J. Liu, J.-G. Zhang, and W. Xu, *Chem*, **4**, 1877 (2018).
- S. Jiao, X. Ren, R. Cao, M. H. Engelhard, Y. Liu, D. Hu, D. Mei, J. Zheng, W. Zhao, Q. Li, N. Liu, B. D. Adams, C. Ma, J. Liu, J.-G. Zhang, and W. Xu, *Nat. Energy*, **3**, 739 (2018).
- Z. Zeng, V. Murugesan, K. S. Han, X. Jiang, Y. Cao, L. Xiao, X. Ai, H. Yang, J.-G. Zhang, M. L. Sushko, and J. Liu, *Nat. Energy*, **3**, 674 (2018).
- J. Alvarado, M. A. Schroeder, T. P. Pollard, X. F. Wang, J. Z. Lee, M. H. Zhang, T. Wynn, M. Ding, O. Borodin, Y. S. Meng, and K. Xu, *Energy & Environmental Science*, **12**, 780 (2019).
- J. Wang, W. Huang, A. Pei, Y. Li, F. Shi, X. Yu, and Y. Cui, *Nat. Energy*, **4**, 664 (2019).
- P. Li, C. Li, Y. Yang, C. Zhang, R. Wang, Y. Liu, Y. Wang, J. Luo, X. Dong, and Y. Xia, *Research*, **2019**, 7481319 (2019).
- S. Ge, Y. Leng, T. Liu, R. S. Longchamps, X. G. Yang, Y. Gao, D. Wang, D. Wang, and C. Y. Wang, *Sci. Adv.*, **6**, eaay7633 (2020).
- J. Xia, L. Madec, L. Ma, L. D. Ellis, W. Qiu, K. J. Nelson, Z. Lu, and J. R. Dahn, *J. Power Sources*, **295**, 203 (2015).
- H.-J. Noh, S. Yoon, C. S. Yoon, and Y.-K. Sun, *J. Power Sources*, **233**, 121 (2013).
- J. Qian, B. D. Adams, J. Zheng, W. Xu, W. A. Henderson, J. Wang, M. E. Bowden, S. Xu, J. Hu, and J.-G. Zhang, *Adv. Funct. Mater.*, **26**, 7094 (2016).

46. B. D. Adams, J. Zheng, X. Ren, W. Xu, and J.-G. Zhang, *Adv. Energy Mater.*, **8**, 1702097 (2018).
47. H.-B. Han, S.-S. Zhou, D.-J. Zhang, S.-W. Feng, L.-F. Li, K. Liu, W.-F. Feng, J. Nie, H. Li, and X.-J. Huang, *J. Power Sources*, **196**, 3623 (2011).
48. R. Jung, M. Metzger, F. Maglia, C. Stinner, and H. A. Gasteiger, *J. Electrochem. Soc.*, **164**, A1361 (2017).
49. R. Jung, P. Strobl, F. Maglia, C. Stinner, and H. A. Gasteiger, *J. Electrochem. Soc.*, **165**, A2869 (2018).
50. Y. Leng, S. Ge, D. Marple, X.-G. Yang, C. Bauer, P. Lamp, and C.-Y. Wang, *J. Electrochem. Soc.*, **164**, A1037 (2017).
51. R. Weber, M. Genovese, A. J. Louli, S. Hames, C. Martin, I. G. Hill, and J. R. Dahn, *Nat. Energy*, **4**, 683 (2019).